PERGAMON

Chemical Engineering Science 56 (2001) 3123–3137

Chemical Engineering Science

www.elsevier.nl/locate/ces

Stability analysis of a pressure swing adsorption process

C. Béchaud[a,b], S. Mélen[c], D. Lasseux[a,*], M. Quintard[d], C. H. Bruneau[b]

[a] *Laboratoire Energétique et Phénomènes de Transfert–UMR 8508, Esplanade des Arts et Métiers, 33405 Talence Cedex, France*
[b] *Laboratoire de Mathématiques Appliquées de Bordeaux-351 Cours de la Libération, 33405 Talence Cedex, France*
[c] *Air Liquide, Centre de Recherche Claude-Delorme–Les Loges en Josas–B.P. 126, 78350 Jouy-en-Josas, France*
[d] *Institut de Mécanique des Fluides de Toulouse–UMR 5502–Allée du Prof. C. Soula, 31400 Toulouse, France*

Received 27 January 2000; received in revised form 7 January 2001; accepted 7 January 2001

Abstract

Hydrodynamic stability during advection combined with diffusion and adsorption of a binary gas mixture in porous media is considered in this work. The general framework is that of pressure swing adsorption (PSA) on beds of zeolite beads. The dispersion/adsorption problem is studied at Darcy's scale on a 1D porous column from a numerical point of view while complete time-periodic cycles are considered. The regular solution of the problem is first sought using a finite volume scheme and stability analysis is performed on this time-dependent solution. While instability evidence is shown on a direct 2D numerical simulation of the problem with pressure and concentration disturbances at the entrance of the column, the stability analysis is carried out in 1D by making use of the linear amplitude equation method. Results clearly show the stability conditions which are quite different depending on whether pressure or concentration disturbances are considered as initial conditions or maintained as boundary conditions at column entrance.

Keywords: Adsorption; Dispersion; Porous media; Stability; Transport processes; Zeolites

1. Introduction

Pressure swing adsorption processes—referred to as PSA in this work—are widely used in a variety of industrial applications like air drying, gas purification, solvent recovery among the principals. For oxygen production from air in particular, this technique offers interesting advantages in terms of energy consumption, as compared to cryogenic processes for instance, and allows on-site installation due to a relatively light infrastructure. Basically, the technique consists in adsorbing nitrogen of air on reactive sites within a porous bed made of zeolite to produce oxygen at the bed outlet.

Originally, PSA is based on the so-called Skarstrom (1959) cycle, even though many other cycles were derived afterwards for performance purposes (Turnock & Kadlec, 1971; Kowler & Kadlec, 1972). The Skarstrom cycle involves two main steps: an adsorption step during which oxygen is actually produced, and a depressurization one which corresponds to a regeneration of the bed. The overall process is characterized by its performance which is usually estimated with the aid of two main parameters: *product recovery* and *adsorbent productivity*. The former represents the concentration ratio between the inlet and outlet of the non-adsorbed component—oxygen for instance—while the latter is the amount of the non-adsorbed component produced per unit of adsorbent. Many studies on the PSA process have been carried out in order to improve its performance. For instance, Turnock and Kadlec (1971) and Kowler and Kadlec (1972) developed a variation of the Skarstrom one-column process (called pressure swing parametric pumping process). This was designed to separate a mixture of nitrogen and methane. They focused their attention on the feed pressure wave-form, and observed experimentally that the optimum feed pressure wave-form was a square one. Considerable improvements of this parametric pumping process, in the case of oxygen and nitrogen separation from air, was obtained later by Jones and Keller (1981) by modifying the time steps in the cycle. Another idea to increase PSA performance has been proposed. It consists in coupling the process with other gas separation techniques. For instance, Vaporciyan and Kadlec (1987, 1989), Lu

* Corresponding author.
E-mail address: lasseux@lept-ensam.u-bordeaux.fr (D. Lasseux).

0009-2509/01/$ - see front matter
PII: S0009-2509(01)00016-1

and Rodrigues (1994) combined chemical reaction to PSA, and Bhaumik, Majumdar, and Sirkar (1996) integrated the best features of membrane contacting, gas liquid absorption and PSA to give rise to the so-called rapid pressure swing absorption (RAPSAB). Other investigations were performed on the PSA performance. Efficiency of various adsorbents, like carbon molecular sieves (CMS) and zeolite, was compared by Farooq and Ruthven (1990). They found that CMS lead to a higher product recovery whereas zeolite productivity is better. For this reason, most of the PSA processes are designed with zeolite as adsorbent material. Later, Lemcoff and Lacava (1992) and Shirley and Lacava (1993) stressed the importance of the regeneration pressure on the performance. Their conclusion was that a better performance is achieved when pressurization is done by feed gas and product backfill. Effects of parameters like "dead" zones, adsorption isotherms, incomplete pressurization and blow-down, as well as feed composition, isothermal or adiabatic operations on the separation performance were investigated by Lu, Loureiro, Rodrigues, and LeVan (1993). They showed that the number of cycles required to achieve the cyclic steady state is shorter in the isothermal case than in the adiabatic one. A recent study of Shirley and Lemcoff (1997) highlighted the effect of cycle time on performance as well as on purity of the product. It was found that performance improves with increasing cycle time especially for high purity whereas purity is independent of cycle time for low purity regimes.

In existing works, two main approaches have been followed to model the process. On the one hand, the pore diffusion model was introduced to represent the intra-particle diffusional mass transfer resistance. This model was used by Yang and Doong (1985), Sun and Meunier (1991) and Lu et al. (1993) to predict concentration evolution during the different steps. On the other hand, a more simplified model, referred to as the linear driving force (LDF) model, has been used. It is based on an approximated description of the flow within the pores, and does not take explicitly into account molecular diffusion (Carter & Wyszynski, 1983). Comparisons between these two models and experimental data were performed by Farooq and Ruthven (1990). Their results indicated that the pore diffusion model provides a better agreement with actual data than the LDF model, in spite of a significantly longer computational time. Differences observed between model predictions and experimental data may result from simplifications involved in the physical model. They may also be explained by additional mechanisms that are not taken into account in these models. Among the most important ones, heterogeneity effects or development of hydrodynamic instabilities may affect dramatically the flow. In this paper, we consider the possible occurrence of instabilities, and we investigate the influence of various physical parameters involved in the process on the development of such instabilities.

Hydrodynamic instabilities have been reported for a long time in the literature in the case of passive dispersion in porous media (see a review by Homsy, 1987), or in the case of the development of a thermal diffusion zone (see Quintard, 1983). Interaction of these instability mechanisms with heterogeneities in the porous bed has also been investigated (Homsy, 1987; Tan & Homsy, 1992). However, occurrence of instabilities during dispersion and adsorption, and for the case of compressible gases, has not been studied so far. In the present work, a stability analysis was performed on the basis of a pore diffusion model used to describe the transport of the two chemical species—oxygen and nitrogen. The regular flow corresponds to the 1D solution of the governing equations. Since our objective is to develop the analysis in the case of PSA processes, the resulting 1D base flow is time-dependent, periodic in time, with a complex evolution due to the periodic change in the boundary conditions. To investigate the stability of this time-dependent solution, a linear amplitude equation associated with 2D inlet perturbations was developed (Quintard, 1983). A numerical model was derived to solve for this amplitude equation. Time evolution of the disturbance amplitude indicates whether instabilities can develop or not. Results allow us to discuss the effect of the perturbation wavelength and amplitude on the development of instabilities.

2. Physical problem

The system under consideration was designed to produce oxygen from air (mixture of 78% nitrogen and 21% oxygen). Air flows within three columns containing a bed of porous zeolite beads. Zeolite adsorb nitrogen more than oxygen. The air-flow cycle under study derives from the Skarstrom cycle, and corresponds to three main steps that are detailed below. To ensure a continuous production (Yang & Doong, 1985), all three columns are used simultaneously, each of them undergoing one cycle step (see Fig. 1).

The three main steps of a cycle correspond to:

(1) adsorption during two distinct periods:
  (I) a feeding period: air is injected and adsorption of nitrogen results in oxygen production;
  (II) a delay period during which adsorption continues while depressurization begins;
(2) purge:
  (III) during this period, the bed is depressurized with the help of a vacuum pump;
(3) pressurization during which one can observe:
  (IV) an elution period which corresponds to a pressurization with gas coming from the bed running in period (II). A consequence of this design is that elution period has the same time length as period II;

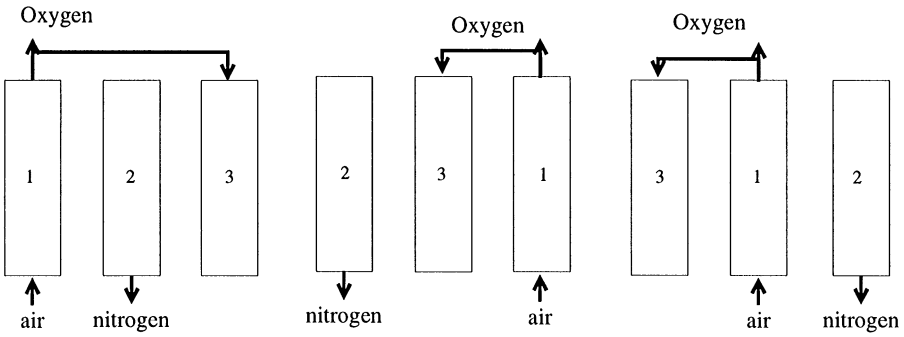

Fig. 1. The three main steps in the adsorption cycle.

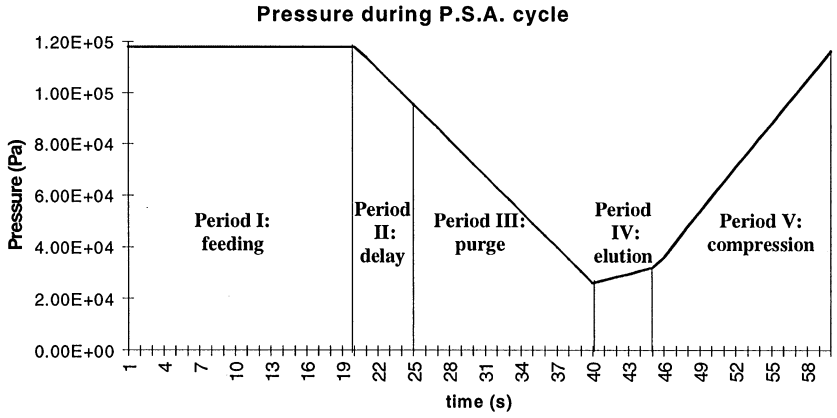

Fig. 2. Entrance pressure evolution during a complete cycle.

(V) a compression period to regenerate the bed using oxygen produced in period (I).

Production of oxygen occurs during the two first periods, while the three other ones are designed to regenerate the bed in order to restore the adsorption capacity of zeolite. The overall process is represented schematically in Fig. 2 where we have represented the evolution of the entrance pressure. It is important to notice that all the three columns are coupled so that gas production at the outlet of one column is used as inlet for another one.

Physical mechanisms in this problem can be considered at many different scales: the pore scale which corresponds to pores within the porous zeolite beads; the macro-pore scale, with a characteristic length of beads diameter; the scale of few beads corresponding to an homogeneous pack which is often referred to as Darcy-scale in the porous media literature; and the mega-scale corresponding to the entire column with packing heterogeneities. In the following, the solution to the stability problem is proposed at the macroscopic-Darcy-scale and equations at this scale are taken from the literature. The problem of deriving these macroscopic equations from some averaging technique applied to the pore-scale equations is beyond the scope of this paper (see, for instance, Whitaker, 1986; Hassanizadeh & Gray, 1979; Quintard & Whitaker, 1994), and they are taken without further discussion. For the initial boundary-value problem, we assume that physical parameters of the porous bed, like porosity, dispersion coefficients, heat capacities and heat conduction coefficients are constant. Since the column diameter is much smaller than its length, the flow problem is considered as 1D and is solved on the homogeneous system schematically depicted in Fig. 3. Because gas phase density is small, gravity is neglected since this type of force is assumed to play a minor role compared to adsorption forces.

The gas phase, or β-phase, is a binary mixture of oxygen, β_1, and nitrogen, β_2, while the solid phase, σ, is assumed to be rigid and immobile. The initial boundary-value problem is given by mass, momentum and energy balance equations, associated with boundary conditions corresponding to the cycle under study. The set of equations are given below.

2.1. Mass balance

Mass balance for component i ($i=\beta_1$ or β_2) in the gas mixture is a convection/dispersion equation with additional terms taking into account gas compressibility and

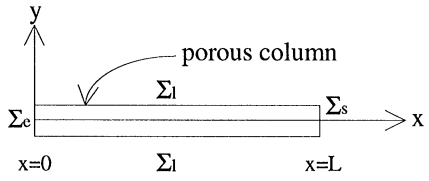

Fig. 3. Geometry of the macroscopic medium.

adsorption. For the oxygen component, this writes

$$\underbrace{\varepsilon\frac{\partial\rho_\beta}{\partial t}C_{\beta_1}+\varepsilon\rho_\beta\frac{\partial C_{\beta_1}}{\partial t}}_{compression}+\underbrace{(1-\varepsilon)\frac{\partial f(C_{\beta_1})}{\partial t}}_{adsorption}+\underbrace{\nabla\cdot(\rho_\beta\mathbf{V}_\beta C_{\beta_1})}_{convection}$$
$$=\underbrace{\nabla\cdot(\rho_\beta\mathbf{D}^*_\beta\cdot\nabla C_{\beta_1})}_{dispersion},\qquad(1)$$

where C_{β_1} is the macroscopic oxygen mass fraction in the gas phase defined by

$$C_{\beta_i}=\frac{m_i}{m},\qquad(2)$$

m_i being the mass of component i $(i=1,2)$ in a mass m of the mixture; $\mathbf{V}_\beta$ and $\mathbf{D}^*_\beta$ are the macroscopic velocity and dispersion tensor; ε is the porosity of the medium and f represents the adsorption isotherm defined below. Rather than writing the equivalent equation for the nitrogen component, it is more convenient to write the total mass balance that results from the sum of Eq. (1) for both components to obtain

$$\underbrace{\varepsilon\frac{\partial\rho_\beta}{\partial t}}_{compressibility}+\underbrace{\nabla\cdot(\rho_\beta\mathbf{V}_\beta)}_{convection}$$
$$=\underbrace{-(1-\varepsilon)\left(\frac{\partial\rho_\sigma C_{\sigma_1}}{\partial t}+\frac{\partial\rho_\sigma C_{\sigma_2}}{\partial t}\right)}_{adsorption},\qquad(3)$$

where C_{σ_1} and C_{σ_2} denote, respectively, the mass of oxygen and nitrogen adsorbed per unit mass of the porous medium.

Adsorption is a physico-chemical phenomenon that depends in a nonlinear way on pressure, temperature and species concentration in the fluid phase. For a given adsorbent, this relationship is generally given under the form of a so-called isotherm, and in the present work, a Langmuir relationship was used. This kind of relationship has proved to be very accurate for the air/zeolite system at low pressure (Van Tassel, Davis, & McCormick, 1994). In addition, we assumed that the macroscopic concentration is equal to the pore-scale equilibrium concentration. This assumption corresponds to a local chemical equilibrium assumption and was discussed in some details by Quintard and Whitaker (1998), and Ahmadi, Quintard, and Whitaker (1998). As a consequence the following Langmuir isotherm was used, which, for component i reads

$$\rho_\sigma C_{\sigma_i}=f(C_{\beta_i})=\frac{\alpha_i\exp(\delta h_i/RT)C^m_{\beta_i}P_\beta}{1+\kappa_i\exp(\delta h_i/RT)C^m_{\beta_i}P_\beta}.\qquad(4)$$

In this isotherm, $C^m_{\beta_i}$ represents the molecular fraction of component i and is given by

$$C^m_{\beta_i}=\frac{n_i}{n_m},\qquad(5)$$

where n_i is the number of molecules of component i contained in a mixture of n_m molecules; δh_i represents the molar enthalpy of adsorption; α_i and κ_i are system dependent constants and R is the ideal gas constant.

2.2. Momentum balance

Provided the pore Reynolds number is less than 10, it is usually admitted that a valid model for momentum conservation in a homogeneous porous medium is the classical Darcy's law. In our case, the Reynolds number estimated from the mean pore diameter and interstitial velocity is below this critical value and consequently, since gravity is neglected, the following relationship was used for the β-phase momentum balance:

$$\mathbf{V}_\beta=-\frac{1}{\mu_\beta}\mathbf{K}\cdot\nabla P_\beta,\qquad(6)$$

where $\mathbf{K}$ is the permeability tensor defined on a homogeneous representative sample of the bed.

2.3. Energy balance

Following some ideas put forth for the local chemical equilibrium assumption, local thermal equilibrium between the gas phase and the solid phase was further assumed (Quintard, Kaviany, & Whitaker, 1997). This yields a unique macroscopic equation to describe the temperature evolution within the fluid–solid system which reads

$$\underbrace{(\rho C_p)^*\frac{\partial T}{\partial t}}_{accumulation\ term}+\underbrace{\nabla\cdot((\rho C_p)_\beta\mathbf{V}_\beta T)}_{convection}=\underbrace{\nabla\cdot(\mathbf{K}^*\cdot\nabla T)}_{heat\ diffusion}$$
$$+\underbrace{(1-\varepsilon)\left(\frac{\partial\rho_\sigma C_{\sigma_1}}{\partial t}\delta h_1+\frac{\partial\rho_\sigma C_{\sigma_2}}{\partial t}\delta h_2\right)}_{adsorption}$$
$$+\underbrace{\varepsilon\frac{\partial P_\beta}{\partial t}+\mathbf{V}_\beta\cdot\nabla P_\beta}_{pressure\ reduction}.\qquad(7)$$

In the above equation, $\mathbf{K}^*$ and $(\rho C_p)^*$ represent the equivalent heat conductivity tensor and the equivalent volumetric heat capacity of the fluid/solid system, respectively. This latter property is defined by a mixing law of the following type:

$$\chi^* = \varepsilon\chi_\beta + (1-\varepsilon)\chi_\sigma. \tag{8}$$

To close the problem, one needs a constitutive equation for the gas phase. For simplicity, an *ideal gas law* was used to define gas density. According to the definitions of the mass fractions of the two components, one obtains the density of the mixture as

$$\rho_\beta = \frac{P_\beta}{[C_{\beta_1}/M_{\beta_1} + (1-C_{\beta_1})/M_{\beta_2}]RT}, \tag{9}$$

where M_{β_i} is the molar mass of component i.

2.4. Initial and boundary conditions

Boundary conditions at entrance, Σ_e, and exit, Σ_s, of one column are those corresponding to the successive periods over a complete cycle. For sake of clarity, they are listed below for each period:

Period I (*feeding*):

(B.C.1) $T(t) = T_e$ on Σ_e, (10)

(B.C.2) $C_{\beta_1}(t) = C_{\beta_{1_e}}$ on Σ_e, (11)

(B.C.3) $P_\beta(t) = P_{\beta_e}$ on Σ_e, (12)

(B.C.4) $P_\beta(t) = P_{\beta_s}$ on Σ_s, (13)

(B.C.5) $\mathbf{n}\cdot\mathbf{K}^*\cdot\nabla T(t) = 0$ on Σ_s, (14)

(B.C.6) $\mathbf{n}\cdot\mathbf{D}^*_\beta\cdot\nabla C_{\beta_1}(t) = 0$ on Σ_s. (15)

Period II (*delay*):

(B.C.7) $\mathbf{V}_\beta(t) = 0$ on Σ_e, (16)

(B.C.8) $\mathbf{n}\cdot\mathbf{K}^*\cdot\nabla T(t) = 0$ on Σ_e, (17)

(B.C.9) $\mathbf{n}\cdot\mathbf{D}^*_\beta\cdot\nabla C_{\beta_1}(t) = 0$ on Σ_e, (18)

(B.C.10) $P_\beta(t) = P_{\beta_s}(t)$ on Σ_s, (19)

(B.C.11) $\mathbf{n}\cdot\mathbf{K}^*\cdot\nabla T(t) = 0$ on Σ_s, (20)

(B.C.12) $\mathbf{n}\cdot\mathbf{D}^*_\beta\cdot\nabla C_{\beta_1}(t) = 0$ on Σ_s. (21)

During this period, $P_{\beta_s}(t)$ corresponds to a fixed linear pressure evolution. Values of $\mathbf{V}_\beta, C_{\beta_1}$ and T over time at the outlet are later used in period IV.

Period III (*depressurization*):

(B.C.13) $P_\beta(t) = P_{\beta_e}(t)$ on Σ_e, (22)

(B.C.14) $\mathbf{n}\cdot\mathbf{K}^*\cdot\nabla T(t) = 0$ on Σ_e, (23)

(B.C.15) $\mathbf{n}\cdot\mathbf{D}^*_\beta\cdot\nabla C_{\beta_1}(t) = 0$ on Σ_e, (24)

(B.C.16) $\mathbf{V}_\beta(t) = 0$ on Σ_s, (25)

(B.C.17) $\mathbf{n}\cdot\mathbf{K}^*\cdot\nabla T(t) = 0$ on Σ_s, (26)

(B.C.18) $\mathbf{n}\cdot\mathbf{D}^*_\beta\cdot\nabla C_{\beta_1}(t) = 0$ on Σ_s. (27)

During this depressurization period, $P_{\beta_e}(t)$ is an imposed linear decreasing function of time.

Period IV (*elution*):

(B.C.19) $P_\beta(t) = P_{\beta_e}(t)$ on Σ_e, (28)

(B.C.20) $\mathbf{n}\cdot\mathbf{K}^*\cdot\nabla T(t) = 0$ on Σ_e, (29)

(B.C.21) $\mathbf{n}\cdot\mathbf{D}^*_\beta\cdot\nabla C_{\beta_1}(t) = 0$ on Σ_e, (30)

(B.C.22) $\mathbf{V}_\beta(t) = 0$ on Σ_s, (31)

(B.C.23) $T(t) = T_s(t)$ on Σ_s, (32)

(B.C.24) $C_{\beta_1}(t) = C_{\beta_{1_s}}(t)$ on Σ_s. (33)

During this period, $P_{\beta_e}(t)$ is an imposed linear increasing function of time and conditions at any time on Σ_s are those corresponding to period II.

Period V (*pressurization*):

(B.C.25) $\mathbf{V}_\beta(t) = 0$ on Σ_e, (34)

(B.C.26) $\mathbf{n}\cdot\mathbf{K}^*\cdot\nabla T(t) = 0$ on Σ_e, (35)

(B.C.27) $\mathbf{n}\cdot\mathbf{D}^*_\beta\cdot\nabla C_{\beta_1}(t) = 0$ on Σ_e, (36)

(B.C.28) $P_\beta(t) = P_{\beta_s}(t)$ on Σ_s, (37)

(B.C.29) $T(t) = T_{\text{initial}}$ on Σ_s, (38)

(B.C.30) $C_{\beta_1}(t) = C_{\beta_{1_{\text{initial}}}}$ on Σ_s. (39)

During this final period, $P_{\beta_s}(t)$ is a fixed linear pressure evolution, whereas oxygen concentration as well as temperature on Σ_s are kept constant and equal to their initial values at the beginning of the cycle.

This initial boundary-value problem was solved numerically and a stability analysis with respect to pressure or concentration perturbations was performed. Methodology and numerical procedures used to compute the regular solution on the β phase pressure, P^0_β, temperature, T, oxygen concentration, $C^0_{\beta_1}$, and velocity, $\mathbf{V}^0_\beta$, as well as the corresponding disturbances are now presented.

3. Hydrodynamic stability

Our study of the hydrodynamic stability of the PSA process under consideration is inspired by techniques developed for the case of miscible displacements (Wooding, 1962; Bachu & Dagan, 1979; Bertin & Quintard, 1984; Tan & Homsy, 1986; Homsy, 1987; Yortsos & Zeybek, 1988; Prouvost & Quintard, 1990) or transient heat diffusion (Gresho & Sani, 1970; Homsy, 1973; Quintard & Prouvost, 1982).

A very popular technique is the classical *bifurcation theory*— or *linear stability analysis*—(Iooss & Joseph, 1980) which is well adapted to the case of autonomous regular solution. In fact, if W^0 denotes the regular solution vector or base state, and w the associated disturbance, then the equations for the disturbance can be linearized in the neighborhood of the regular solution and formally written as

$$\frac{\partial w(\mathbf{x},t)}{\partial t} = \mathbf{L}(w(\mathbf{x},t), W^0(\mathbf{x})), \tag{40}$$

where $\mathbf{L}$ is the linear operator and W^0 the regular solution which is a function of the spatial coordinates, $\mathbf{x}$, only. The stability analysis can be performed by studying the behavior of the operator $\mathbf{L}$ with respect to an elementary perturbation of the form:

$$w(\mathbf{x},t) = \mathrm{e}^{\alpha t}\varphi(\mathbf{x}), \tag{41}$$

which implies

$$\alpha\varphi(\mathbf{x}) = \mathbf{L}(\varphi(\mathbf{x}), W^0), \tag{42}$$

where α and φ are, respectively, eigenvalues and eigenvectors of the operator $\mathbf{L}$. Marginal stability is obtained for values of the physical parameters such that $\alpha = 0$.

In our case, however, the regular solution (we also used the term *base flow*) is time dependent in a complex non-linear fashion and the resulting disturbance equations lead to a non-autonomous system. A non-autonomous system is characterized by the fact that coefficients in the disturbance equations are time dependent while the regular solution is a non-stationary one. For this kind of system, more complex approaches are required (Homsy, 1973, 1987; Quintard, 1983, 1984; Tan & Homsy, 1986, 1992; Yortsos & Zeybek, 1988) like the frozen time method, the linear amplitude equation method or the energy method that are very briefly presented below.

(i) *Frozen time or quasi-static or quasi-steady-state analysis*. As mentioned above, the bifurcation theory between steady-state flows is no longer valid when W is a function of space and time. However, assuming that t is a parameter in $W(\mathbf{x},t)$,—this is a strong hypothesis in this theory and is difficult to justify—the base flow concentration field becomes *frozen*, and the linear analysis can be formally applied to the disturbances. A lot of stability studies (Foster, 1965; Robinson, 1967; Gresho & Sani, 1970; Tan & Homsy, 1986) have been based on this method since it is easier to implement than the two other methods described below. However, it is of limited usefulness for most transient cases. In particular, the marginal stability, which corresponds to zero time derivative for the disturbance is certainly the worst situation compared to the finite time variations of the base flow. Therefore, it is better to use the conditions for rapid disturbance growth as instability criteria (Tan & Homsy, 1986). However, in our case the base state is periodic in time, with complex variations due to the various changes in the boundary conditions. Therefore, it is difficult to estimate the validity conditions for this quasi-steady-state approach.

(ii) *Linear amplitude equation method*. Linear amplitude equations can be derived from the original governing equations in the case of non-autonomous systems. Solutions of the resulting equations give valuable information about the possible development of perturbations and, in this respect, yields better results than the previous theory. However, it is not suitable for describing well-developed perturbations, which can interact in a non-linear fashion (Malher, Schechter, & Wissler, 1968; Quintard, 1983).

(iii) *Energy method*. This method can account for well-developed perturbations (Joseph, 1976; Homsy, 1973). In order to determine the stability conditions, a Liapounov functional is built from the governing equations. This method is interesting since non-linearities present in the system are taken into account. In particular, this method can show how a perturbation can actually vanish when combined with time evolution of the regular solution while it is considered as an unstable one for the two other methods (Quintard, 1984). In other words, this analysis provides critical times at which perturbations may increase or decrease depending on the evolution of the base flow and other parameters (Quintard & Prouvost, 1982). However, it might be difficult to obtain the solution in the case of very complicated problems, i.e., many coupled, non-linear equations. Therefore, the effect of the non-linearities is often investigated by solving the full set of non-linear equations for various disturbance patterns. This is used to validate the conclusions of the stability analyses. However, it generally requires heavy computations, and cannot be used for a parametric study.

Because of the cyclic nature and the complexity of the system under study in the present work, linear amplitude equations were derived and solved numerically for the stability analysis. To simplify the mathematical treatment of the problem, we assumed that the temperature disturbance has a negligible effect on the overall stability. This implies that the energy equation will not be considered in the stability analysis, i.e., it will be reduced to Darcy's law combined with the mass conservation.

In the following, we use P^0_β, T, $C^0_{\beta_1}$ and $\mathbf{V}^0_\beta$ for the solution to the base flow corresponding to the initial boundary-value problem described by Eqs. (1)–(30). The disturbance fields, $\tilde{P}_\beta, \tilde{\mathbf{V}}_\beta, \tilde{C}_\beta$, are defined as

$$\tilde{P}_\beta = P_\beta - P^0_\beta, \tag{43}$$

$$\tilde{C}_{\beta_1} = C_{\beta_1} - C^0_{\beta_1}, \tag{44}$$

$$\tilde{\mathbf{V}}_\beta = \mathbf{V}_\beta - \mathbf{V}^0_\beta. \tag{45}$$

The disturbance linearized equations were obtained by introducing these decompositions into the governing equations, Eqs. (1)–(7). During the linearization process, products of disturbances of the form $\tilde{X}_\beta \tilde{Y}_\beta$ were discarded and the following disturbance equations were obtained:

Darcy's law:

$$\tilde{\mathbf{V}}_\beta = -\frac{1}{\mu_\beta}\mathbf{K}\cdot\nabla\tilde{P}_\beta. \tag{46}$$

Oxygen mass balance:

$$\underbrace{\varepsilon\left(\rho^0_\beta\frac{\partial\tilde{C}_{\beta_1}}{\partial t}+\tilde{\rho}_\beta\frac{\partial C^0_{\beta_1}}{\partial t}\right)+\varepsilon\left(\frac{\partial\rho^0_\beta}{\partial t}\tilde{C}_{\beta_1}+\frac{\partial\tilde{\rho}_\beta}{\partial t}C^0_{\beta_1}\right)}_{compression}$$
$$+\underbrace{(1-\varepsilon)\left(\frac{\partial\tilde{f}\,(C_{\beta_1})}{\partial t}\right)}_{adsorption}$$
$$-\underbrace{\nabla\cdot(\rho^0_\beta\mathbf{D}^*_\beta\cdot\nabla\tilde{C}_{\beta_1})}_{dispersion}$$
$$=-\underbrace{\nabla\cdot(\rho^0_\beta\mathbf{V}^0_\beta\tilde{C}_{\beta_1})-\nabla\cdot(\rho^0_\beta\tilde{\mathbf{V}}_\beta C^0_{\beta_1})}_{convection}. \tag{47}$$

Mass balance for the mixture:

$$\underbrace{\varepsilon\left(\frac{\partial\tilde{\rho}_\beta}{\partial t}\right)}_{compression}+\nabla\cdot\underbrace{(\rho^0_\beta\tilde{\mathbf{V}}_\beta+\tilde{\rho}_\beta\mathbf{V}^0_\beta)}_{convection}$$
$$+\underbrace{(1-\varepsilon)\left(\frac{\partial\tilde{f}(C_{\beta_1})}{\partial t}+\frac{\partial\tilde{f}(C_{\beta_2})}{\partial t}\right)}_{adsorption}=0. \tag{48}$$

In the two above equations, a series of approximations were used. In particular, adsorption and compressibility terms were developed on the basis of the following Taylor's expansions:

$$\rho_\beta=\rho^0_\beta+\underbrace{\left.\frac{\partial\rho_\beta}{\partial C_{\beta_1}}\right|_{C^0_{\beta_1},P^0_\beta}\tilde{C}_{\beta_1}+\left.\frac{\partial\rho_\beta}{\partial P_\beta}\right|_{C^0_{\beta_1},P^0_\beta}\tilde{P}_\beta+\cdots}_{\tilde{\rho}_\beta} \tag{49}$$

$$f(C_{\beta_i})=f^0(C_{\beta_i})+\underbrace{\left.\frac{\partial f(C_{\beta_i})}{\partial C_{\beta_i}}\right|_{C^0_{\beta_i},P^0_\beta}\tilde{C}_{\beta_i}+\left.\frac{\partial f(C_{\beta_i})}{\partial P_\beta}\right|_{C^0_{\beta_i},P^0_\beta}\tilde{P}_\beta+\ldots}_{\tilde{f}(C_{\beta_i})} \tag{50}$$

in which higher second-order terms were neglected. Moreover, in Eq. (47), the following inequalities were assumed in order to simplify the dispersive and convective terms:

$$\nabla\cdot\left(\left(\left.\frac{\partial\rho_\beta}{\partial C_{\beta_1}}\right|_{C^0_{\beta_1},P^0_\beta}\tilde{C}_{\beta_1}+\left.\frac{\partial\rho_\beta}{\partial P_\beta}\right|_{C^0_{\beta_1},P^0_\beta}\tilde{P}_\beta\right)\mathbf{D}^*_\beta\cdot\nabla C^0_{\beta_1}\right)$$
$$\ll\nabla\cdot(\rho^0_\beta\mathbf{D}^*_\beta\cdot\nabla\tilde{C}_{\beta_1}), \tag{51}$$

$$\nabla\cdot\left(\left(\left.\frac{\partial\rho_\beta}{\partial C_{\beta_1}}\right|_{C^0_{\beta_1},P^0_\beta}\tilde{C}_{\beta_1}+\left.\frac{\partial\rho_\beta}{\partial P_\beta}\right|_{C^0_{\beta_1},P^0_\beta}\tilde{P}_\beta\right)\mathbf{V}^0_\beta C^0_{\beta_1}\right)$$
$$\ll\nabla\cdot(\rho^0_\beta\mathbf{V}^0_\beta\tilde{C}_{\beta_1}). \tag{52}$$

Physically, this corresponds to the hypothesis of a negligible density disturbance with respect to the concentration and pressure disturbances. This leads to

$$\nabla\cdot\left(\left(\left.\frac{\partial\rho_\beta}{\partial C_{\beta_1}}\right|_{C^0_{\beta_1},P^0_\beta}\tilde{C}_{\beta_1}+\left.\frac{\partial\rho_\beta}{\partial P_\beta}\right|_{C^0_{\beta_1},P^0_\beta}\tilde{P}_\beta\right)\mathbf{D}^*_\beta\cdot\nabla C^0_{\beta_1}\right)$$
$$\approx 0, \tag{53}$$

$$\nabla\cdot\left(\left(\left.\frac{\partial\rho_\beta}{\partial C_{\beta_1}}\right|_{C^0_{\beta_1},P^0_\beta}\tilde{C}_{\beta_1}+\left.\frac{\partial\rho_\beta}{\partial P_\beta}\right|_{C^0_{\beta_1},P^0_\beta}\tilde{P}_\beta\right)\mathbf{V}^0_\beta C^0_{\beta_1}\right)\approx 0 \tag{54}$$

in Eq. (48).

Since the base flow is assumed to be one-dimensional, and due to the structure of the operator, it is possible to decompose the pressure and concentration disturbances under the form

$$\tilde{C}_{\beta_1}(t,x,y)=\bar{C}(t,x)g(y), \tag{55}$$

$$\tilde{P}_\beta(t,x,y)=\bar{P}(t,x)g(y). \tag{56}$$

Once inserted in the linearized equations, this implies that

$$\nabla^2_y g+a^2 g=0, \tag{57}$$

in which a is a constant. Since the system can be considered as infinite in the y-direction, an elementary solution for g is hence,

$$g(y)=\sin\left(\frac{2\pi}{\lambda}y\right) \tag{58}$$

and a can be identified to the wave number as

$$a = \frac{2\pi}{\lambda}. \tag{59}$$

3.1. Initial and boundary conditions

To complete the system of equations, Eqs. (46)–(48), initial and boundary conditions are required and their choice is of capital interest in the stability analysis of non-autonomous systems. In fact, in the case of classical bifurcations between steady solutions, it is sufficient to know that perturbations exist. If the system is under unstable conditions, the solution eventually switch from the stable base flow to another solution and the structure of the perturbed state does not often depend on the choice of the initial disturbance. Physically, this means that the source of the instability is irrelevant for the analysis. This statement has to be slightly moderated, however, in the case of sub-critical conditions since the jump from one solution to another may depend in that case upon the disturbance amplitude. This is much more complicated when the system is non-autonomous. The behavior of the system is highly dependent on sources giving rise to the perturbations. For instance, in the case of the stability of transient thermal diffusion zones in porous media, it was found that the observed critical times depend on the choice of the initial perturbations (Quintard, 1984). In some cases for which the diffusion zone is convected through the porous medium, i.e. a base flow with a non-zero velocity, the perturbation seems to be of limited growth compared to the case of a stagnant zone if we observe the flow over a limited length. This is simply because convection flushes the disturbance away from the domain before it has reached a finite amplitude accessible to observation (Quintard, Bertin, & Prouvost, 1987). All these aspects are illustrated and discussed below with the presentation of results on the particular problem studied in this paper.

From a mathematical point of view, several different choices are possible for the perturbation sources. For instance, the source may be an initial perturbation of finite amplitude. If the system is unstable for the conditions under study, we may observe an increase in the perturbation amplitude. However, and this is especially true for cyclic conditions, the disturbance may be carried away from the domain under consideration by convection, and if there is no source associated with the boundary conditions the disturbances will eventually vanish. Subsequently, there will be virtually no perturbation sources for the following cycles. In a real system, perturbation may originate from sources that do not support the scheme of a field only perturbed initially. For instance, if the perturbation is initiated by small fluctuations of physical properties—like heterogeneities—one can easily imagine that this perturbation is kept all along the cycle and not only at the early stage of the flow. For this reason, a stationary disturbance could be maintained for instance at the entrance, in addition to an initial perturbation. Alternatively, a perturbation could be superimposed to the solution at each time step in a random manner. This last idea was not investigated in the present work and results obtained in the case of an initial perturbation on the one hand and for a stationary disturbance at the boundary on the other hand are presented. This allows the discussion of the stability problem on a general basis keeping in mind that detailed practical applications would require more knowledge of the possible perturbation sources.

Stationary boundary conditions of the perturbed problem were taken similar to the boundary conditions of the regular problem. For instance, Neuman conditions for the regular concentration, Eqs. (15), (18), (21), (24), (27), (30) and (36), remain Neuman conditions for the disturbed fields, while Dirichlet conditions for regular concentration and regular pressure, Eqs. (11)–(13), (19), (22), (28), (33), (37) and (39), remain Dirichlet conditions. These Dirichlet conditions were prescribed as follows

$$\text{(B.C.31)} \quad \tilde{C}_{\beta_1}(t,y) = 0 \quad \text{on } \Sigma_e \text{ (Period I)}, \tag{60}$$

$$\text{(B.C.32)} \quad \tilde{C}_{\beta_1}(t,y) = 0 \quad \text{on } \Sigma_s \text{ (Periods IV, V)}, \tag{61}$$

$$\text{(B.C.33)} \quad \tilde{P}_{\beta}(t,y) = \bar{P}(t,x)\sin\left(\frac{2\pi}{\lambda}y\right) \text{ on } \Sigma_e \text{ (Periods I, III, IV)}, \tag{62}$$

$$\text{(B.C.34)} \quad \tilde{P}_{\beta}(t,y) = 0 \quad \text{on } \Sigma_s \text{ (Periods I, II, V)}, \tag{63}$$

where Σ_e and Σ_s represent the entrance and exit surfaces. The boundary condition in Eq. (62) takes into account pressure fluctuations occurring at the entrance of the domain. In the case of impervious boundaries, the regular velocity is zero, as expressed by the boundary conditions in Eqs. (16), (25), (31), (34), and this implies that the pressure perturbation is also equal to zero.

In the case of an initial perturbation field, two different concentration conditions were investigated: an over-oxygenation and an under-oxygenation.

4. Discretization and numerical procedure

A classical finite volume method was used to solve the regular problem, Eqs. (1), (3), (4), (6), (7) and (9), and the perturbed one, Eqs. (46)–(48), with their corresponding boundary conditions. Integration was performed on the control volume depicted in Fig. 4 where we have also indicated the positions of the unknowns.

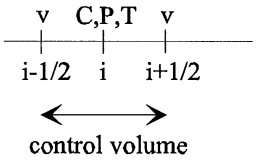

Fig. 4. Control volume.

The base flow and disturbed problems are coupled and involve seven unknowns, $P^0_\beta, \tilde{P}_\beta, C^0_{\beta_1}, \tilde{C}_{\beta_1}, \mathbf{V}^0_\beta, \tilde{\mathbf{V}}_\beta$ and T, which must be computed at the same time step. To do so, convective, dispersive and accumulation terms present in each set of equations were, respectively, discretized according to a specific scheme. Convective (or hyperbolic) terms, like $\nabla \cdot (\rho_\beta \mathbf{V}_\beta C_{\beta_1})$ and $\nabla \cdot ((\rho C_p)_\beta \mathbf{V}_\beta T)$, were discretized using an explicit upwind first-order and conservative scheme. The explicit formulation was chosen in order to get a linear form of the problems, and moreover, to provide an efficient way of limiting numerical diffusion. Diffusive (or elliptic) terms $\nabla \cdot (\rho_\beta \mathbf{D}^*_\beta \cdot \nabla C_{\beta_1})$ and $\nabla \cdot (\mathbf{K}^* \cdot \nabla T)$ were discretized with an implicit scheme based on second-order centered finite differences. Accumulation terms including compressibility and adsorption effects, $\partial \rho_\beta / \partial t$ and $\partial \rho_\sigma C_{\sigma_1} / \partial t$, respectively, were discretized according to the following scheme:

$$\frac{\partial \rho_\beta}{\partial t} = \left(\frac{\partial \rho_\beta}{\partial C_{\beta_1}}\right)^n \frac{\partial C_{\beta_1}}{\partial t} + \left(\frac{\partial \rho_\beta}{\partial P_\beta}\right)^n \frac{\partial P_\beta}{\partial t} + \left(\frac{\partial \rho_\beta}{\partial T}\right)^n \frac{\partial T}{\partial t}. \tag{64}$$

As a result, the discretized form of Eq. (1), for instance, reads

$$\begin{aligned}
&\varepsilon \left(\left[\frac{\partial \rho_\beta}{\partial C_{\beta_1}}\right]_i^n \frac{(\delta C_{\beta_1})_i}{\delta t} + \left[\frac{\partial \rho_\beta}{\partial P_\beta}\right]_i^n \frac{(\delta P_\beta)_i}{\delta t} \right. \\
&\left. + \left[\frac{\partial \rho_\beta}{\partial T}\right]_i^n \frac{(\delta T)_i}{\delta t} \right) (C_{\beta_1})_i^n + \varepsilon (\rho_\beta)_i^n \frac{(\delta C_{\beta_1})_i}{\delta t} \\
&+ (1-\varepsilon) \left\{ \left[\frac{\partial f(C_{\beta_1})}{\partial C_{\beta_1}}\right]_i^n \frac{(\delta C_{\beta_1})_i}{\delta t} + \left[\frac{\partial f(C_{\beta_1})}{\partial P_\beta}\right]_i^n \frac{(\delta P_\beta)_i}{\delta t} \right. \\
&\left. + \left[\frac{\partial f(C_{\beta_1})}{\partial T}\right]_i^n \frac{(\delta T)_i}{\delta t} \right\} \\
&- (\rho_\beta)_i^n D^*_\beta \frac{(C_{\beta_1})_{i+1}^{n+1} - 2(C_{\beta_1})_i^{n+1} + (C_{\beta_1})_{i-1}^{n+1}}{\delta x^2} \\
&= - (\rho_\beta)_i^n \begin{cases} (\mathbf{V}_\beta)^n_{i+1/2} (C_{\beta_1})^n_i & \text{if } (\mathbf{V}_\beta)^n_{i+1/2} > 0, \\ (\mathbf{V}_\beta)^n_{i+1/2} (C_{\beta_1})^n_{i+1} & \text{if } (\mathbf{V}_\beta)^n_{i+1/2} < 0, \\ -(\mathbf{V}_\beta)^n_{i-1/2} (C_{\beta_1})^n_{i-1} & \text{if } (\mathbf{V}_\beta)^n_{i-1/2} > 0, \\ -(\mathbf{V}_\beta)^n_{i-1/2} (C_{\beta_1})^n_i & \text{if } (\mathbf{V}_\beta)^n_{i-1/2} < 0, \end{cases}
\end{aligned} \tag{65}$$

Table 1
Values of the physical parameters

D^*_β	$1.5 \times 10^{-5}\,\mathrm{m^2/s}$
$\mathbf{K}$	$2.43 \times 10^{-9}\,\mathrm{m^2}$
$\mathbf{K}^*$	$0.78\,\mathrm{W\,m^{-1}\,K^{-1}}$
$(\rho C_p)^*$	$41.5 \times 10^4\,\mathrm{J\,kg^{-1}\,K^{-1}}$

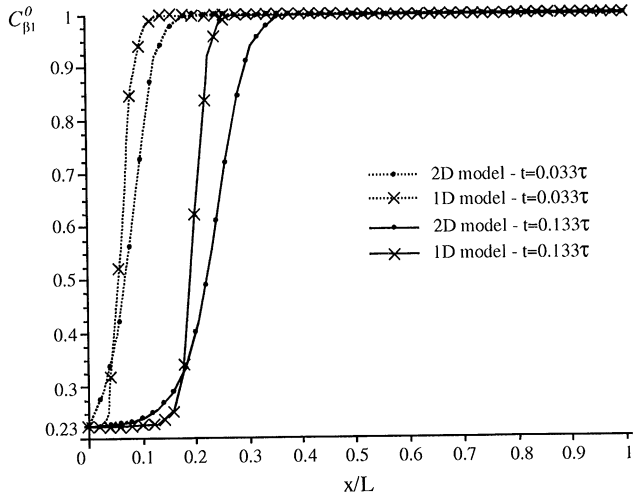

Fig. 5. Regular solution, oxygen mass fraction profiles along the column as obtained by the 1D and 2D models during the feeding period; $\mathrm{V}_\beta = 5.004 L/\tau$.

where the notations $(\delta C_{\beta_1})_i/\delta t$, $(\delta P_\beta)_i/\delta t$ and $(\delta T)_i/\delta t$ were used to represent $[(C_{\beta_1})_i^{n+1} - (C_{\beta_1})_i^n]/\delta t$, $[(P_\beta)_i^{n+1} - (P_\beta)_i^n]/\delta t$, and $[(T)_i^{n+1} - (T)_i^n]/\delta t$, respectively.

For the perturbed problem, the integration of $\nabla \cdot (\rho^0_\beta \mathbf{D}^*_\beta \cdot \nabla \tilde{C}_{\beta 1})$ and $\nabla \cdot (\rho^0_\beta \mathbf{K} \cdot \nabla \tilde{P}_\beta)$ generates additional source terms of the form $a^2 \tilde{C}_{\beta_1}$ and $a^2 \tilde{P}_{\beta_1}$ as a result of the decomposition in Eqs. (55) and (56), and these terms were discretized by an explicit scheme.

For each problem, unknowns were computed as the solution of the linear system formed from the set of linearized discrete equations using a classical Gauss elimination method.

5. Results and discussion

In all our results presented below, length and time are made dimensionless by the column length, L, and complete cycle time, τ, respectively. Computations were performed using the values of the physical parameters reported in Table 1.

5.1. Regular case

To begin with, the 1D base flow was solved using the above-mentioned numerical scheme. In Fig. 5, we have

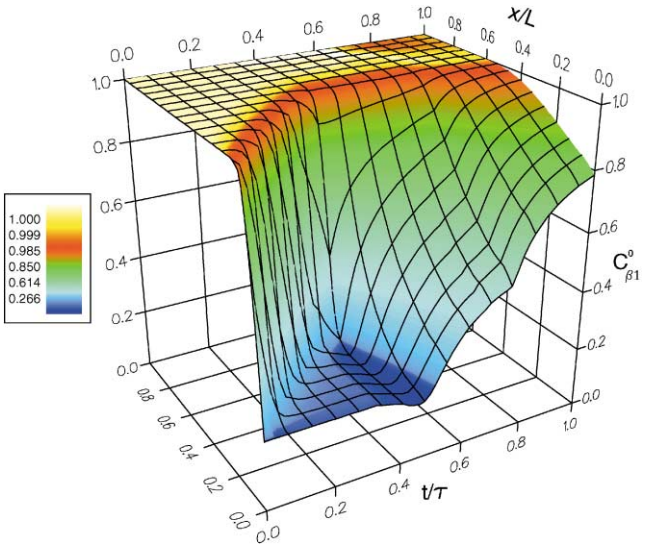

Fig. 6. Regular oxygen mass fraction along the column over a complete cycle.

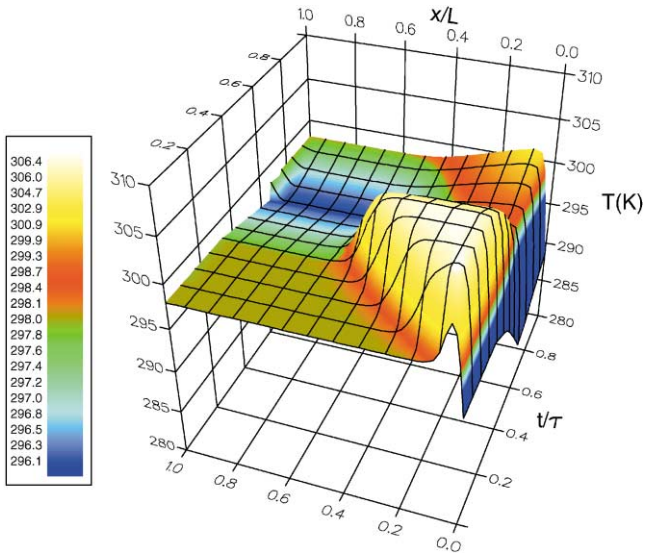

Fig. 7. Regular temperature along the column over a complete cycle.

represented the results for concentration versus the dimensionless position along the porous column axis. These results were obtained during the feeding period after a dimensionless time of 0.033 and 0.133 in the first cycle. As a comparison, the regular solution was also computed using a 2D numerical model [1] over the same period of time and concentration results obtained at a fixed value of y corresponding to the mid-section are also depicted in Fig. 5.

One can observe a small difference between the two adsorption waves due to the fact that the 2D numerical model takes into account the time to reach adsorption equilibrium, i.e., it uses a local non-equilibrium model, whereas adsorption equilibrium is assumed to be instantaneous in the 1D model. However, the agreement between the two approaches is good, and the regular solution obtained from the 1D model was considered to be accurate enough for the subsequent stability analysis. For the same flow rate, results on oxygen mass fraction and temperature evolution over a complete cycle are represented in Figs. 6 and 7 versus dimensionless time and position along the column axis, respectively.

To complete the regular flow analysis, it is also necessary to test the effect of the cyclic nature of the process on the regular solution. Results on the regular concentration evolutions along the porous column during the early stage of the feeding period over four cycles are depicted in Fig. 8. They indicate that:

(i) A cyclic steady state is reached after few cycles (typically 2 or 3) depending on the flow rate. This is in agreement with previous reported results obtained under isothermal conditions (Lu et al., 1993). As a consequence, cyclic steady-state conditions are considered as initial conditions in the subsequent stability analysis.

(ii) The porous bed recovery decreases with increasing flow rate.

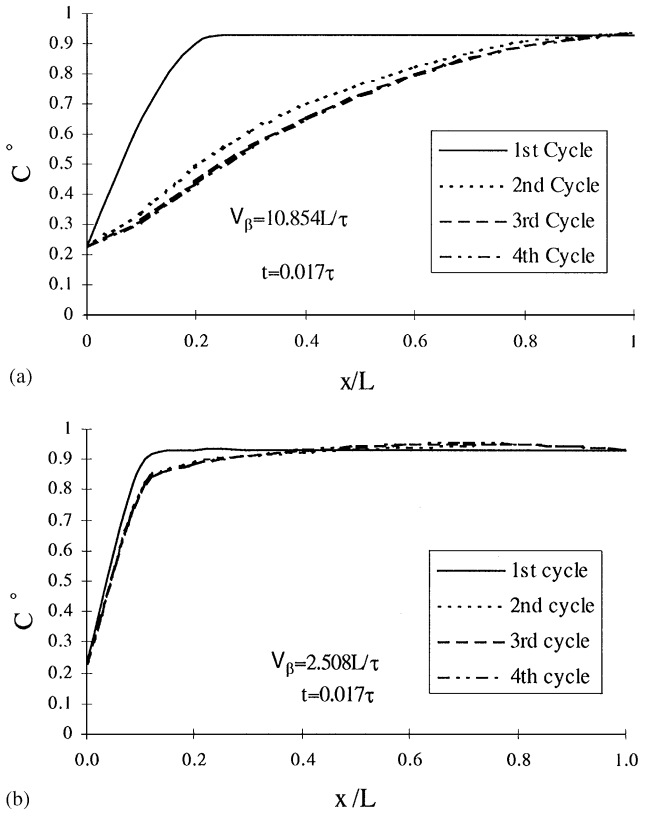

Fig. 8. Regular concentration evolution along the porous column at the early stage of feeding for four cycles and two different flow rates. (a) $V_\beta = 10.854L/\tau$; (b) $V_\beta = 2.508L/\tau$.

[1] The 2D numerical model was developed in RAMPANT™ by Fluent Inc..

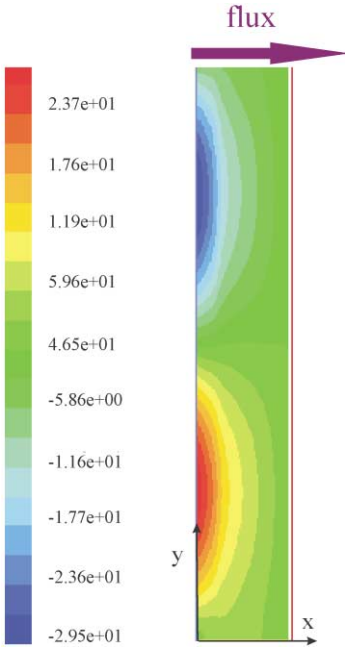

Fig. 9. Simulation with a 2D model: perturbed pressure in the porous medium; $t = 0.133\tau$; $V_\beta = 2.508L/\tau$.

(iii) Steady state is reached more rapidly for low flow rates. In practice, however, gas production rate may require high flow rates despite lower ones are in favor of higher bed recovery and earlier steady state.

Starting from these results, the perturbed equations were solved according to the scheme described above.

5.2. Perturbed case

Before presenting our results, it is important to emphasize that the unstable behavior is intrinsic of the system under consideration and is not a pure artifact resulting from the 1D linearization of the system of equations. As an illustration, a 2D numerical solution was obtained on the feeding period using RAMPANT^{TM} with a perturbation for the pressure boundary condition given, as in Eq. (62), by

$$\tilde{P}_\beta(t, x = 0, y) = \bar{P} \sin\left(\frac{2\pi}{\lambda} y\right), \tag{66}$$

and a concentration initial perturbation of the form:

$$\tilde{C}_{\beta_1}(t = 0, x, y) = \bar{C} x(L - x) \sin\left(\frac{2\pi}{\lambda} y\right), \quad 0 \leqslant x \leqslant L. \tag{67}$$

Pressure results obtained with $\bar{P} = 20$ Pa, $\lambda = L$ and $\bar{C} = 0.05$ at $t = 0.133\tau$ during the feeding period are reported in Fig. 9.

Clearly, the perturbation grows and spreads inside the porous column confirming that disturbances may develop inside the medium and justifying a more thorough computation over a complete cycle with the 1D simplified model.

To begin with, perturbed equations were solved with an initial concentration perturbation only, i.e., $\bar{P} = 0$, and no disturbances applied on the boundaries. Two different types of concentration perturbations were investigated: one corresponding to an over-oxygenation of the column, the other one to an under-oxygenation. Both disturbance fields were of the form given in Eq. (67). Computation was performed on the overall cycle and results obtained with $\bar{C} = \pm 0.05$ and $\lambda = L$ are reported in Fig. 10 were we have represented the time evolution, over the five periods, of the relative norm of the oxygen concentration, $\|\tilde{C}_{\beta_1}(t)\|_{r,2}$, defined by

$$\|\tilde{C}_{\beta_1}(t)\|_{r,2} = \frac{\|\tilde{C}_{\beta_1}(t)\|_2}{\|\tilde{C}_{\beta_1}(t = 0)\|_2} = \frac{\sqrt{\int_0^L \tilde{C}^2_{\beta_1}(x, t)\,\mathrm{d}x}}{\sqrt{\int_0^L \tilde{C}^2_{\beta_1}(x, t = 0)\,\mathrm{d}x}}. \tag{68}$$

It is clear from these results that the perturbation evolution differs from step to step and depends on the initial perturbation. During purge and delay, the perturbed concentration increases, whatever the initial perturbation. During elution and pressurization steps the perturbed concentration decreases. On the contrary, one can observe a different behavior during the feeding period since perturbation increases with an over-oxygenation while it decreases with an under-oxygenation. Although its evolution depends on the velocity inside the column, (see results in Fig. 11 for $\bar{C} = -0.05$ and two different flow rates), perturbations are always dampened after few steps.

In fact, in this problem, perturbations are carried away from the porous medium by convection while a zero perturbation condition at the inlet tends to be convected into the porous domain since there is no perturbation maintained at the inlet. Therefore, since we are considering a cyclic behavior it is expected that the system is relatively stable. Here the word stable has to be understood in terms of transient analysis. Indeed, several calculations showed that the flow is stable with these boundary conditions and for the physical situation under consideration, whatever the initial concentration perturbation and the wave number. In terms of practical applications, such a situation may seem to be too drastic. In order to release this constraint, it is interesting to investigate the case of a perturbation maintained at the inlet of the column. This kind of condition is physically justified by experimental observations of velocity fluctuations at the entrance during feeding, purge and elution steps.

Computations were performed with a perturbed pressure boundary condition of the form given in Eq. (62). Results on $\|\tilde{C}_{\beta_1}(t)\|_{r,2}$ versus dimensionless time obtained with a fixed wavelength, λ, equal to L, and $\bar{P}$ ranging from 5 to 30 Pa are represented in Fig. 12. These results

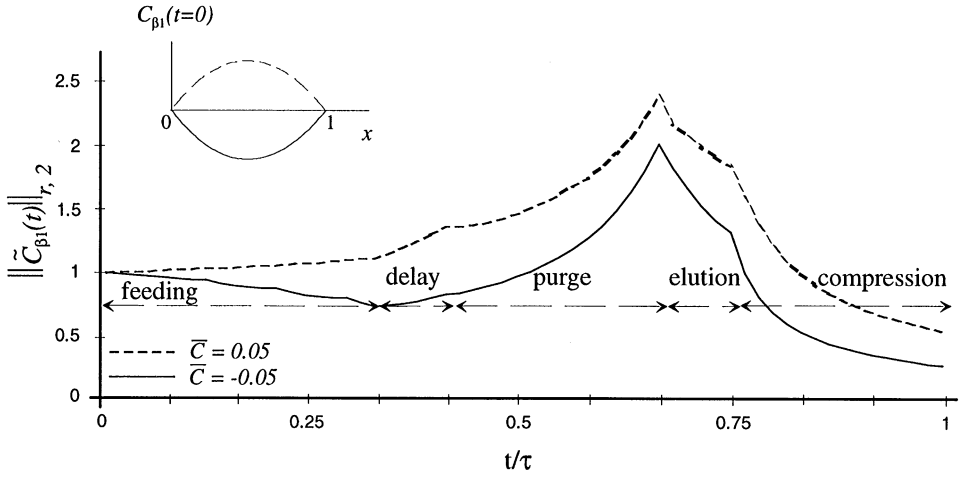

Fig. 10. Evolution of the relative norm of the perturbed concentration over one cycle resulting from initial concentration perturbations; $V_\beta = 2.508\,L/\tau$.

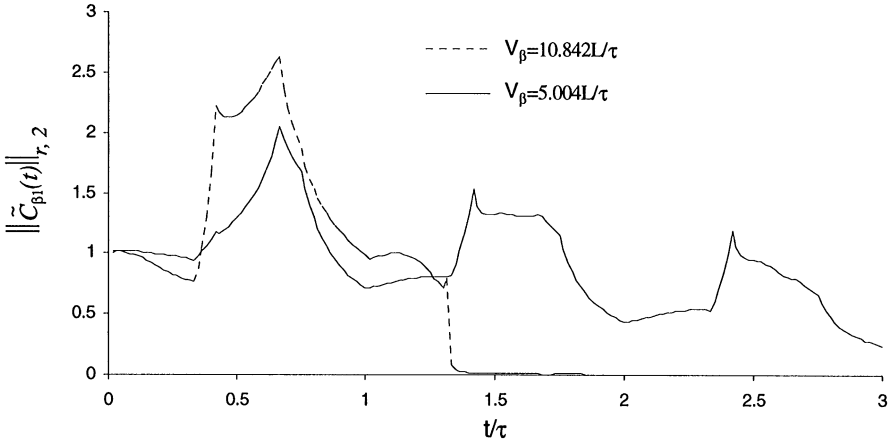

Fig. 11. Evolution of the relative norm of the perturbed concentration along the column for an initial under-oxygenation and two different flow rates.

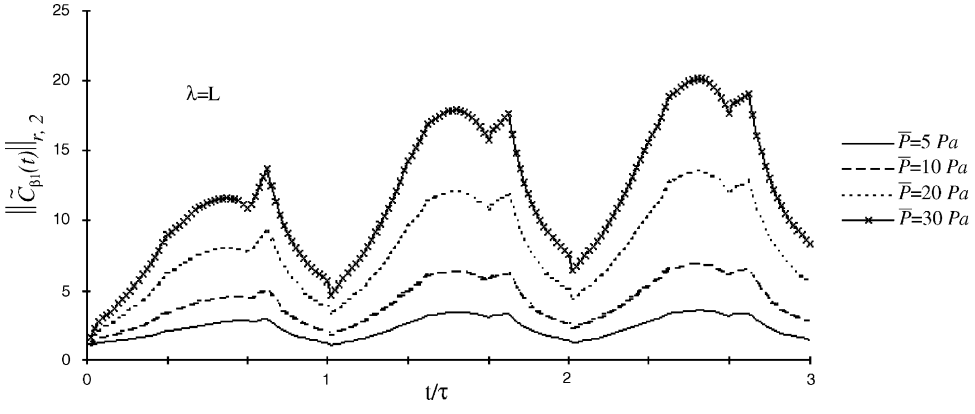

Fig. 12. Evolution of the relative norm of the perturbed concentration resulting from a perturbed pressure at the entrance. Effect of the perturbation amplitude.

clearly highlight the conditional stability of the system. For this wavelength, for instance, the concentration disturbance begins to grow for an amplitude of the pressure perturbation greater than 5 Pa.

However, disturbance amplitude at the entrance is not the only factor influencing stability since the wavelength is also a key factor conditioning the stability. In Fig. 13, are reported our results for $\|\tilde{C}_{\beta_1}(t)\|_{r,2}$ versus

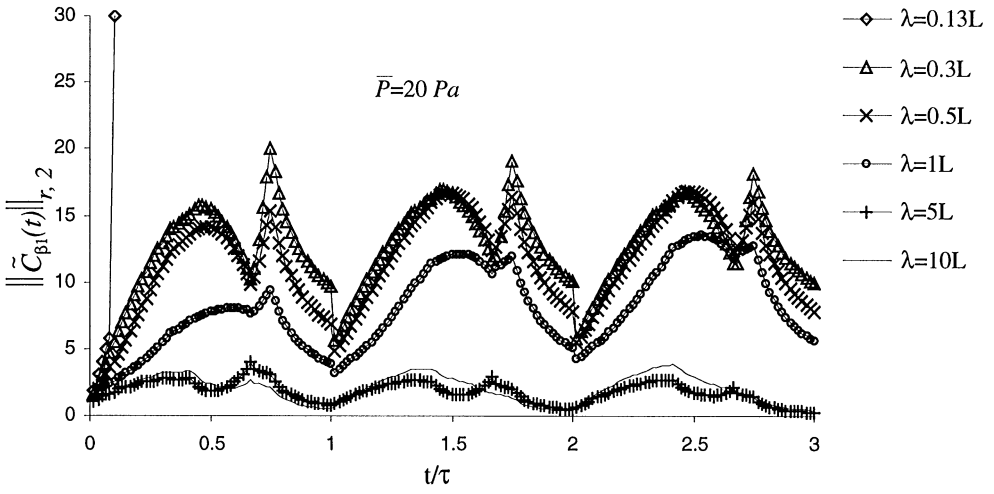

Fig. 13. Evolution of the relative norm of the concentration disturbance resulting from a perturbed pressure at the entrance. Effect of the perturbation wavelength.

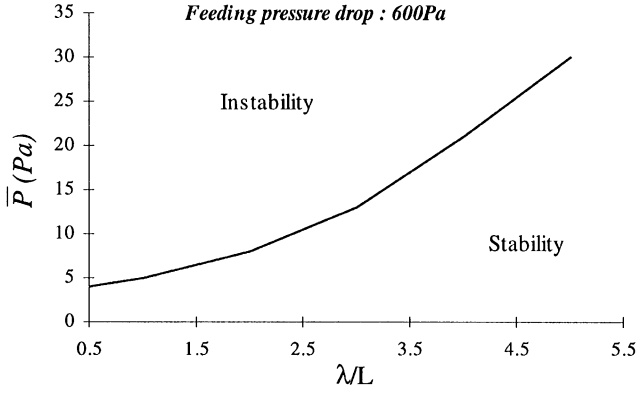

Fig. 14. Hydrodynamic stability threshold as a function of the disturbance wavelength and amplitude, for a fixed feeding pressure drop.

dimensionless time, obtained with the inlet pressure disturbance amplitude fixed to 20 Pa and wavelengths ranging from $0.13 \times L$ to $10 \times L$. These results indicate that stability occurs for relatively large wavelengths (roughly larger than $5L$ in our case), while the time to reach the instability decreases with decreasing wavelengths. For very short wavelengths, the solution diverges very quickly and this directly results from the linear character of the operator.

To synthesize the above results, we have summarized the stability analysis in Fig. 14 providing the stability diagram in terms of amplitude and wavelength of the pressure disturbance at the entrance of the column. This diagram was obtained for a pressure drop of 600 Pa along the column during the feeding period.

As shown in this figure, unstable flow results from large enough disturbance amplitudes at the entrance, i.e., for a sufficiently large amount of energy input in the system. The amount of energy required to reach this unstable behavior is an increasing function of the wavelength.

6. Conclusions

In this work, stability during cyclic gas flow with dispersion and adsorption in a porous column, as encountered during pressure swing adsorption, was investigated. On the basis of a 1D linearized amplitude equation, and from the computed solution of the time-dependent regular flow, a numerical solution was obtained for the concentration perturbation in the case of two different kinds of disturbance. For an initial concentration disturbance, it was found that the system is always stable. This result can be explained if one considers the effect of convection through the porous domain. In fact, since no disturbance is maintained at the entrance, a zero disturbance tends to be convected through the column so that the initial disturbance is finally dampened away. A somewhat different behavior was observed if a perturbation is maintained at the inlet for the pressure boundary condition for instance. In this case a conditional stability is obtained on the adsorption front inside the porous medium. It was found that instability occurs for large enough perturbation amplitude at the inlet, and that the amplitude required to destabilize the dispersion/adsorption process increases with increasing wavelengths. Although the influence of all the physical parameters has not been investigated since it was beyond our scope in the present work, a stability diagram in terms of amplitude and wavelength of the pressure perturbation at the inlet was obtained.

Notation

a	wave number, rad/m
C_{β_i}	total mass fraction of oxygen ($i=1$) or nitrogen ($i=2$) in the gas phase β
$C^0_{\beta_i}$	regular mass fraction for component i in the gas phase β
$\tilde{C}_{\beta_i}$	perturbed mass fraction for component i in the gas phase β
$C^m_{\beta_i}$	molar fraction of component i
C_{σ_i}	mass fraction of component i in the solid phase σ
$\mathbf{D}^*_\beta$	dispersion coefficient in the gas phase, m^2/s. Here, $\mathbf{D}^*_\beta = D^*_\beta \mathbf{I}$
$f(C_{\beta_i})$	function describing the adsorption isotherm for component i
$\mathbf{K}$	porous media permeability, m^2. Here, $\mathbf{K} = K\mathbf{I}$
$\mathbf{K}^*$	thermal conductivity of the fluid/solid system, $W/m\,K^{-1}$. Here, $\mathbf{K}^* = K^*\mathbf{I}$
L	column length, m
m_i	mass of component i in a mass m of mixture, kg
m	mass of the gas mixture, kg
M_{β_i}	molar mass of component i, kg/mol
n_i	number of molecules of component i contained in a mixture of n_m molecules
n_m	number of molecules in the gas mixture
P_β	gas pressure, N/m^2
P^0_β	gas pressure, N/m^2 (base flow)
$\tilde{P}_\beta$	disturbed gas pressure, N/m^2
R	ideal gas constant, $J/mol\,K^{-1}$
t	time, s
T	temperature of the fluid/solid system, K
$\mathbf{V}_\beta$	gas filtration velocity, m/s
$\mathbf{V}^0_\beta$	gas filtration velocity, m/s (base flow)
$\tilde{\mathbf{V}}_\beta$	disturbed gas filtration velocity, m/s

Greek letters

α_i	adsorption constant for component i, $(m/s)^{-2}$
ε	porous medium porosity
δh_i	adsorption enthalpy between the two phases for component i, J/mol
κ_i	adsorption constant for component i, $(N/m^2)^{-1}$
λ	disturbance wavelength, m
μ_β	gas dynamic viscosity, $N/m^2\,s$
ρ_β	gas density, kg/m^3
ρ_σ	solid density, kg/m^3
$(\rho C_p)^*$	volumetric heat capacity of the fluid/solid system, $J/m^3\,K^{-1}$
$(\rho C_p)_\chi$	volumetric heat capacity of the fluid $-\chi=\beta$- or solid $-\chi=\sigma$- phase, $J/m^3\,K^{-1}$
τ	complete cycle time, s
Σ_e, Σ_s	entrance and exit surfaces of the bed

Acknowledgements

Financial support from the Air Liquide Company is gratefully acknowledged.

References

Ahmadi, A., Quintard, M., & Whitaker, S. (1998). Transport in chemically and mechanically heterogeneous porous media V: Two-equation model for solute transport with adsorption. *Advances in Water Resource*, *22*(1), 59–86.

Bachu, S., & Dagan, G. (1979). Stability of displacement of a cold fluid by a hot fluid in a porous medium. *Physics of Fluids*, *22*(1), 54–59.

Bertin, H., & Quintard, M. (1984). Stabilité d'un écoulement miscible radial en milieu poreux: Étude théorique et expérimentale. *Revue de l'Iinstitut Français du Pétrole*, *39*(5), 573–587.

Bhaumik, S., Majumdar, S., & Sirkar, K. K. (1996). Hollow-fiber membrane-based rapid pressure swing adsorption. *A.I.Ch.E. Journal*, *42*(2), 409–421.

Carter, J., & Wyszynski, M. L. (1983). The pressure swing adsorption drying of compressed air. *Chemical Engineering Science*, *38*(7), 1093–1099.

Farooq, S., & Ruthven, D. M. (1990). A comparison of linear driving force and pore diffusion models for a pressure swing adsorption bulk separation process. *Chemical Engineering Science*, *45*(1), 107–115.

Foster, T. D. (1965). Stability of homogeneous fluid cooled uniformly from above. *Physics of Fluids*, *8*, 1249–1257.

Gresho, P. M., & Sani, R. L. (1970). The stability of a fluid layer subjected to a step change in temperature: Transient vs. frozen time analyses. *International Journal of Heat and Mass Transfer*, *14*, 207–221.

Hassanizadeh, S. M., & Gray, W. G. (1979). General conservation equations for multi-phase systems: 2. Mass, momentum, energy and entropy equations. *Advances in Water Resource*, *2*, 131–141.

Homsy, G. M. (1973). Global stability of time-dependent flows: Impulsively heated or cooled fluid layers. *Journal of Fluid Mechanics*, *60*(1), 129–139.

Homsy, G. M. (1987). Viscous fingering in porous media. *Annual Review of Fluid Mechanics*, *19*, 271–311.

Iooss, G., & Joseph, D. D. (1980). *Elementary stability and bifurcation theory*. New York: Springer.

Jones, R. L., & Keller, G. E. (1981). Pressure swing parametric pumping—a new adsorption process. *Journal of Separation Processing Technology*, *2*(3), 17–23.

Joseph, D. D. (1976). *Stability of fluid motions*. New York: Springer.

Kowler, D. E., & Kadlec, R. H. (1972). The optimal control of a periodic adsorber. *A.I.Ch.E. Journal*, *18*(1), 1207–1219.

Lemcoff, N. O., & Lacava, A. I. (1992). Effect of regeneration pressure level in kinetically controlled pressure swing adsorption. *Gas Separation Purification*, *6*(1), 9–14.

Lu, Z. P., & Rodrigues, A. E. (1994). Pressure swing adsorption reactors: Simulation of three-step one-bed process. *A.I.Ch.E. Journal*, *40*(7), 1118–1137.

Lu, Z. P., Loureiro, J. M., Rodrigues, A. E., & LeVan, M. D. (1993). Simulation of a three-step one-column pressure swing adsorption process. *A.I.Ch.E. Journal*, *39*(9), 1483.

Malher, E. G., Schechter, R. S., & Wissler, E. H. (1968). Stability of a fluid layer with time dependent density gradients. *Physics of Fluids*, *11*(9), 1901–1912.

Prouvost, L., & Quintard, M. (1990). Stability criteria for the design of graded polymer buffers. *Journal of Petroleum Science and Engineering*, *3*(4), 333–343.

Quintard, M. (1983). Stabilité d'une zone instationnaire de diffusion thermique dans un milieu poreux: Analyse linéaire, modélisation numérique. *Journal de Mécanique Théorique et Appliquée*, *2*(5), 751–768.

Quintard, M. (1984). Convection naturelle en milieu poreux: Systèmes non-stationnaires, déplacements. *Annales des Mines*, *5*(6), 85–92.

Quintard, M., Bertin, H., & Prouvost, L. (1987). Criteria for the stability of miscible displacements through porous columns. *Chemie Ingenieur- Technik*, *59*(4), 354–355.

Quintard, M., Kaviany, M., & Whitaker, S. (1997). Two-medium treatment of heat transfer in porous media: Numerical results for effective properties. *Advances in Water Resource*, *20*(2–3), 77–94.

Quintard, M., & Prouvost, L. (1982). Instabilités de zones de diffusion thermique instationnaires en milieu poreux. *International Journal of Heat and Mass Transfer*, *25*(1), 37–44.

Quintard, M., & Whitaker, S. (1994). Convection, dispersion and interfacial transport of contaminants: Homogeneous porous media. *Advances in Water Resource*, *17*, 221–239.

Quintard, M., & Whitaker, S. (1998). Transport in chemically and mechanically heterogeneous porous media IV: Large-scale mass equilibrium for solute transport with adsorption. *Advances in Water Resource*, *22*(1), 33–57.

Shirley, A. I., & Lacava, A. I. (1993). Novel pressurization methods in pressure swing adsorption systems for the generation of high purity gas. *Industrial Engineering & Chemical Research*, *32*, 906–910.

Shirley, A. I., & Lemcoff, N. O. (1997). High-purity nitrogen by pressure-swing adsorption. *A.I.Ch.E. Journal*, *43*(2), 419–424.

Skarstrom, C. W. (1959). Use of adsorption phenomena in automatic plant-type gas analysers. *Annales of the New York Academy of Sciences*, *72*, 751.

Sun, L. M., & Meunier, F. (1991). An improved finite difference method for fixed-bed multicomponent sorption. *A.I.Ch.E. Journal*, *37*(2), 244–254.

Tan, C.-T., & Homsy, G. M. (1986). Stability of miscible displacements in porous media: Rectilinear flow. *Physics of Fluids*, *29*(11), 3549–3556.

Tan, C.-T., & Homsy, G. M. (1992). Viscous fingering with permeability heterogeneity. *Physics of Fluids A*, *4*(6), 1099–1101.

Turnock, P. H., & Kadlec, R. H. (1971). Separation of nitrogen and methane via periodic adsorption. *A.I.Ch.E. Journal*, *17*(2), 335–343.

Van Tassel, P. R., Davis, H. T., & McCormick, A. V. (1994). New lattice model for adsorption of small molecules in zeolite micropores. *A.I.Ch.E. Journal*, *40*(6), 925–934.

Vaporciyan, G. G., & Kadlec, R. H. (1987). Equilibrium-limited periodic separating reactors. *A.I.Ch.E. Journal*, *33*(8), 1334–1343.

Vaporciyan, G. G., & Kadlec, R. H. (1989). Periodic separating reactors: Experiments and theory. *A.I.Ch.E. Journal*, *35*(5), 831–844.

Whitaker, S. (1986). Flow in porous media. I: A theoretical derivation of Darcy's law. *Transport In Porous Media*, *1*, 3–25.

Wooding, R. A. (1962). The stability of an interface between miscible fluids in a porous medium. *Angewandte Mathematik Physik*, *XIII*(3), 183–192.

Yang, R. T., & Doong, S. J. (1985). Gas separation by pressure swing adsorption: A pore-diffusion model for bulk separation. *A.I.Ch.E. Journal*, *31*(11), 1829–1842.

Yortsos, Y. C., & Zeybek, M. (1988). Dispersion driven instability in miscible displacement in porous media. *Physics of Fluids*, *31*(12), 3511–3518.